Progress In Electromagnetics Research, Vol. 108, 155–175, 2010

A COMPARATIVE STUDY ON ISAR IMAGING ALGORITHMS FOR RADAR TARGET IDENTIFICATION

J.-I. Park and K.-T. Kim

Department of Electronic Engineering
Yeungnam University
Gyeongsan, Gyeongbuk, Korea

Abstract—Inverse synthetic aperture radar (ISAR) images represent the two-dimensional (2-D) spatial distribution of the radar cross-section (RCS) of an object and, thus, they can be applied to the problem of target identification. The traditional approach to ISAR imaging is the range-Doppler algorithm based on the 2-D Fourier transform. However, the 2-D Fourier transform often results in poor resolution ISAR images, especially when the measured frequency bandwidth and angular region are limited. Instead of the Fourier transform, high resolution spectral estimation techniques can be adopted to improve the resolution of ISAR images. These are the autoregressive (AR) model, multiple signal classification (MUSIC), and matrix enhancement and matrix pencil MUSIC (MEMP-MUSIC). In this study, the ISAR images from these high-resolution spectral estimators, as well as the FFT approach, are identified using a recently developed identification algorithm based on the polar mapping of ISAR images. In addition, each ISAR imaging algorithm is analyzed and compared in the framework of radar target identification. The results show that the dynamic range as well as the resolution of the ISAR images plays an important role in the identification performance. Moreover, the optimum size of the subarray (i.e., covariance matrix) for MUSIC and MEMP-MUSIC in terms of target identification is experimentally derived.

Received 19 July 2010, Accepted 7 September 2010, Scheduled 14 September 2010
Corresponding author: K.-T. Kim (juniorf@yumail.ac.kr).

1. INTRODUCTION

The problem of reliably identifying aerospace objects has been a matter of primary concern in the field of radar [1–9]. The identification of radar targets can be achieved using various radar signatures, such as natural frequencies, high resolution range (HRR) profiles and inverse synthetic aperture radar (ISAR) images. Natural frequencies due to the resonance phenomena of a target are insensitive to its relative orientation, resulting in radar target identification with robust features [10–13]. However, in a real situation with noise and clutter signals, as well as the target signals, the accurate estimation of these natural frequencies is hard to achieve because their information is included in the late time responses, which are easily corrupted by noise and clutter [14–16]. In contrast, the early time portions of the received signals, i.e., the so-called HRR profiles, are very robust to noise and clutter, but are highly sensitive to the relative aspect angle between the radar and target. ISAR images are not only less sensitive to the relative orientation than the HRR profiles, but are also very immune to noise and clutter, because the coherent integration of the received signals across various aspect angles effectively increases the signal to noise ratio (SNR). Recent advances in ISAR imaging techniques can be found in [17–23].

ISAR images are usually obtained by the range-Doppler algorithm based on the 2-D Fourier transform to convert the data in the spatial frequency domain to reflectivity information in the spatial domain. When the target is moving, a priori processing, such as range alignment and phase adjustment, must be performed before the 2-D Fourier transform, in order to eliminate the translational motion component of the target. In this paper, we assume that the translation motion compensation process is already performed. The Fourier transform is very efficient in terms of computation, because it is implemented using the fast Fourier transform (FFT), but its resolution capability is limited by the spectral bandwidth of the received radar signals. Because the frequency bandwidth and aspect angle region of the received signals are directly proportional to their spectral bandwidth, high resolution ISAR images based on the FFT require advanced radar systems with a wide frequency bandwidth and a long coherent processing interval (CPI).

While high resolution ISAR images with advanced radar systems can achieve high identification performance, there are more cost effective solutions which achieve the same goal. These are high resolution spectral estimation techniques, such as the autoregressive (AR) model, multiple signal classification (MUSIC), and matrix

enhancement and matrix pencil MUSIC (MEMP-MUSIC). Although there are various methods of high resolution spectral analysis, three techniques, viz. the AR model, MUSIC, and MEMP-MUSIC, are considered in this study, because the estimation of the continuous power spectral density (PSD) of the underlying signals is required to produce ISAR images. The estimation of the discrete PSD of the underlying signals is usually achieved via parametric spectral estimation techniques, such as the nonlinear least squares (NLS) method [24], root-MUSIC [24, 25], and ESPRIT (estimation of signal parameters via rotational invariance technique) [24, 26]. The estimated discrete PSD of the radar signal is usually exploited to find the 2-D locations of the high energy scattering centers on the target and associated RCS. In this study, the estimation of only the continuous PSD is considered.

At the cost of additional computation time, these techniques can improve the resolution of ISAR images compared to that of the FFT. The additional computational burden comes from the eigenvalue decomposition of the covariance matrix of received signals. The resolution capability of high resolution spectral estimators depends on the size of the covariance matrix, which is often called the subarray dimension in MUSIC and MEMP-MUSIC, and the model order in the AR model. As the size of the covariance matrix increases, the resolution of the ISAR images improves, due to the increased spectral bandwidth, and vice versa. However, the number of subarrays used to estimate the covariance matrix becomes smaller as its size increases, giving rise to the degradation of the estimation accuracy of the covariance matrix. The estimation accuracy of the covariance matrix has a direct impact on the variance of the estimated PSD, e.g., the dynamic range, of the ISAR images. The dynamic range is defined as the range of pixel amplitudes in a 2-D image, and it has usually been used as an image quality indicator, together with the resolution, in the image processing community. Instead of the dynamic range, a similar metric called the image contrast can be used to measure the quality of ISAR images but, in this study, the simple dynamic range rather than the contrast is exploited. The dynamic range is formally written as follows:

$$\text{Dynamic range} = 20\log_{10}P_{\max} - 20\log_{10}P_{\min} = 20\log_{10}\frac{P_{\max}}{P_{\min}} \quad (1)$$

where $P_{\max}$ and $P_{\min}$ are the maximum and minimum intensity values in linear scales in the ISAR image, respectively.

As the number of average overlapped subarrays becomes smaller, the dynamic ranges of the resulting ISAR images become smaller, implying that the distinction between the target response

and background response resulting from clutter or noise becomes ambiguous, lowering the dynamic ranges. In general, a smaller computation time is preferred for real-time operation and, thus, a smaller subarray dimension can meet this time requirement with the additional benefits of improved dynamic range, but with the drawback of the degraded resolution of the ISAR images. Therefore, for efficient radar target identification, there are two conflicting conditions in the selection of the subarray or model order size, i.e., the resolution and dynamic range.

In this study, we analyze and compare the performance of the previous ISAR imaging methods, the AR model, MUSIC and MEMP-MUSIC, as well as the conventional FFT, for radar target identification. For this purpose, the recently developed identification algorithm based on the polar mapping of ISAR images is combined with the four different techniques. In addition, the optimum subarray size for radar target identification is experimentally determined.

In Section 2, the signal model and four different ISAR imaging techniques are discussed, and also the classifier based on the polar mapping of ISAR images is briefly reviewed. Identification experiments and the associated results will be provided in Section 3, followed by our conclusion in Section 4.

2. ISAR IMAGING AND ISAR IDENTIFICATION METHOD

2.1. Signal Model

The received echo signal $y(f, \theta)$ of a target at frequency f and aspect angle θ can be expressed as follows:

$$y(f,\theta) = \sum_{k=1}^{L} a_k \exp\left(-j\frac{4\pi f}{c}(x_k \cos\theta + y_k \sin\theta)\right) + u(f,\theta) \qquad (2)$$

where L is the number of scattering centers on the target, a_k is the amplitude of the k-th scattering center, and (x_k, y_k) is the position of the k-th scattering center in the spatial domain. u is the additive white Gaussian noise (AWGN) with zero mean and variance σ^2 and c is the speed of light.

The received RCS data uniformly sampled in the frequency-aspect domain (f, θ) does not correspond to the uniformly sampled data in the spatial frequency domain, because (f, θ) and (f_x, f_y) are related by $f_x = \frac{2f}{c}\cos\theta$ and $f_y = \frac{2f}{c}\sin\theta$. Data uniformity in the spatial frequency domain (f_x, f_y) is essential for Fourier transform or high resolution PSD estimators. Therefore, in order to generate

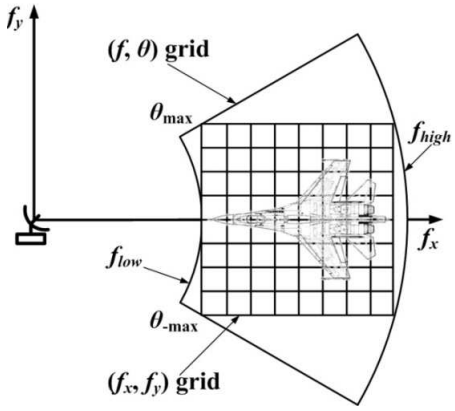

Figure 1. Polar reformatting from (f, θ) domain to (f_x, f_y) domain.

a focused ISAR image, the received data should be converted from polar-formatted samples to Cartesian-formatted samples with uniform spatial frequency sampling spacings, Δf_x and Δf_y, before applying the Fourier transform or high resolution PSD estimation. After polar reformatting as shown Figure 1, the discrete version of the Equation (2) is given by

$$y(m,n) = \sum_{k=1}^{L} a_k \exp\left(-j2\pi(x_k f_x(m) + y_k f_y(n))\right) + u(m,n) \qquad (3)$$

where

$$f_x(m) = f_x(0) + m\Delta f_x, \quad m = 1, 2, \ldots, M,$$
$$f_y(n) = f_y(0) + n\Delta f_y, \quad n = 1, 2, \ldots N,$$

and M and N are the number of interpolated data samples in f_x and f_y respectively.

2.2. ISAR Imaging Based on FFT

After polar reformatting, the spatial reflectivity function of the target can be easily reconstructed by means of a 2-D Fourier transform implemented by a 2-D FFT. The down-range and cross-range resolutions are inversely proportional to the spatial frequency bandwidths, $M\Delta f_x$ and $N\Delta f_y$, respectively. In order to increase the spatial frequency bandwidths, $M\Delta f_x$ and $N\Delta f_y$, for high resolution ISAR images, the frequency bandwidth of the interrogating radar system and relative angular motion between the radar and target

should be sufficiently large. Otherwise, the FFT method results in limited resolution ISAR images, causing unreliable identification performance. Instead of the FFT, high resolution spectral estimation techniques, which will be discussed below, can substantially improve the resolution capability of ISAR images, even with limited data in the (f, θ) domain, at the cost of additional computation time.

2.3. ISAR Imaging Based on AR Model

High resolution 2-D ISAR images can also be generated using an autoregressive model. This method is based on the 2-D forward and backward linear prediction [27]:

$$P_{\mathrm{AR}}(x,y) = \frac{1}{\left|1 + \sum_{\substack{i=0 \\ i=j\neq 0}}^{L}\sum_{j=0}^{L} a_{ij} z_1^{-i} z_2^{-j}\right|^2 + \left|1 + \sum_{\substack{i=0 \\ i=j\neq 0}}^{L}\sum_{j=0}^{L} b_{ij} z_1^{-i} z_2^{-j}\right|^2} \tag{4}$$

$$z_1 = \exp(j4\pi/c\Delta f_x \cdot x), \quad z_2 = \exp(j4\pi/c\Delta f_y \cdot y),$$

where a_{ij} and b_{ij} are the AR coefficients and L is the AR model order. These coefficients can be calculated using forward-backward linear prediction and a least square solution. The function $P_{\mathrm{AR}}(x,y)$ will have sharp peaks at the locations of the scattering centers on the target [27, 28]. However, the function $P_{\mathrm{AR}}(x,y)$ may have more peaks than the number of scattering centers. One can reduce the number of spurious peaks by the singular value decomposition (SVD) of the covariance matrix estimated from the received data. This can be achieved by including only those signal eigenvectors associated with the largest eigenvalues [27, 28].

2.4. ISAR Imaging Based on Spectral MUSIC

To obtain high resolution ISAR images based on MUSIC, the covariance matrix should be estimated from the received data. The eigenvectors of the covariance matrix can be decomposed into the signal subspace eigenvectors and noise subspace eigenvectors. The spectral MUSIC algorithm is based on the orthogonal relationship between the signal and the noise eigenvectors of the covariance matrix. Therefore, the location of the peaks can be estimated using the following function [29]:

$$P_{\mathrm{MUSIC}}(x,y) = \frac{\mathbf{e}(x,y)^H \mathbf{e}(x,y)}{\mathbf{e}(x,y)^H \mathbf{E}_n^H \mathbf{E}_n \mathbf{e}(x,y)}, \tag{5}$$

where $\mathbf{e}(x, y)$ is the mode (direction) vector of the signal subspace, the matrix $\mathbf{E}_n$ is composed of the noise eigenvectors corresponding to the smallest eigenvalues of the covariance matrix, and H denotes the conjugate transpose.

2.5. ISAR Imaging Based on MEMP-MUSIC

It is noted that the rank condition of the covariance matrix can be significantly improved via the matrix enhancement and matrix pencil (MEMP) method based on the Hankel block matrices described in [30], compared to that of the conventional method based on the 2-D modified spatial smoothing preprocessing method described in [29]. The improved covariance matrix can be combined with the MUSIC PSD estimator described in (5), providing more robust ISAR images.

2.6. Identification Method

In this study, the method based on the polar mapping of ISAR images described in [5] was used to identify various ISAR images from six different targets measured in compact range. The method in [5] has the benefits of rotation, scale, and translation invariance, which can mitigate the sensitivity of the ISAR image to the relative orientation, cross-range scaling, and segmentation. In addition, this method is a three step classifier consisting of a coarse search, fine search, and alignment and final decision. After the polar mapping of the ISAR images, each step makes use of its own identification strategy based on the r-projected 1-D image, θ-projected 1-D image, and compressed polar image via principal component analysis (PCA) [31–34]. Even though three feature components are required to complete the identification, the whole memory storage required for the training database is much smaller than that in the case where the original ISAR images are used. As a result, this method was shown to provide more robust identification performance, compared to the conventional template matching with ISAR images [5].

3. EXPERIMENTAL RESULTS

In order to generate the ISAR images, we used six aircraft models with a scale factor of 1/16: The F4, F14, F16, F22, F117 and Mig 29. The maximum length of these targets is about 1 [m].

Their RCS data were measured in a compact range using six scaled models with a frequency bandwidth of the X-band (8.3 GHz $\sim$ 12.3 GHz) in 401 equally spaced frequency points and an angular region

of 180° ($-90° \sim +90°$) in 361 equally spaced angles. The transmit and receive polarizations are chosen as horizontal. An additive white Gaussian noise (AWGN) at a signal-to-noise ratio (SNR) of 30 dB was added to the measured RCS data. The noise added RCS data to which the noise was added was interpolated by polar reformatting. Consequently, 181 ISAR images of 100×100 pixels were generated for each target, providing $181 \times 6 = 1086$ ISAR images for the six target models. In this experiment, we assumed that the translational motion of each target has been perfectly compensated.

To carry out the identification simulation, the 1086 ISAR images were divided into the training set and test set. For this purpose, the training set of each target was uniformly sampled across the aspect angle with an increment of 10°. The rest of the ISAR images were reserved for the test set, i.e., 978 test ISAR images. Every test ISAR image was arbitrarily rotated and down-scaled in order to model the variation of the relative orientation and cross-range scaling of the target. Specifically, its rotation angle and scale are randomly sampled from a uniform distribution between 0 and 2π, and between 1 and $\sqrt{2}$, respectively. The correct identification performance is measured by determining the ratio of the number of correct identifications to the total number of test data.

$$P_c = \frac{\text{the number of correct identification}}{\text{the number of all test set}} \tag{6}$$

Polar images with a size of 50×50 pixels were generated from the ISAR images having sizes of 100×100 pixels and, then, the r-projected 1-D images, the θ-projected 1-D images, and the compressed polar images by PCA were obtained from the polar images. Their dimensions are selected as 50, 50 and 20, respectively, and, thus, the final feature dimensionality for identification is $50 + 50 + 20 = 120$, which is a significantly smaller number than that of the ISAR image itself, 10^4. In addition, in order to investigate the effect of the subarray (model order) size on the identification performance, 10 Monte Carlo identification experiments were carried out at 30 dB. All programs were written in Matlab 6.4 and run in Window XP on Intel Pentium 2.8 GHz processor.

3.1. Experiment 1 — Identification Using Wideband Data

The RCS data for each target with a wide frequency bandwidth of 4 GHz (8.3 GHz $\sim$ 12.3 GHz) and an angular sector of 30° ($-15° \sim +15°$) with respect to the center of each angular sector were used to generate the training and testing ISAR images against the various targets. Note that the target response in the HRR profiles is

represented by about 27 range bins with a frequency bandwidth of 4 GHz, yielding a range resolution of 3.75 cm. The range resolution of 3.75 cm against merely about 1 m target corresponds to 0.6 m range resolution against a real target of 16 m in length. That is, the 4 GHz frequency bandwidth in the experiment is equivalent to the frequency bandwidth of 250 MHz in a real situation, when considering the scale factor.

After adding an AWGN of 30 dB to the measured RCS data, the number of interpolations for polar reformatting was chosen as $M = N = 60$, providing 60 equally spaced data points in both directions, f_x and f_y. Subsequently, the FFT, AR model, MUSIC and MEMP-MUSIC techniques for ISAR imaging were applied to these wide bandwidth-angular sector RCS data.

Figure 2 shows the ISAR image of the F117 scaled model with various spectral estimation techniques when the subarray size for MUSIC and MEMP-MUSIC, and the model order for AR model were chosen as 20. As shown in Figure 2, the dynamic ranges of the ISAR images using the various techniques are 40 dB (FFT), 31.3 dB (MUSIC), 26.2 dB (MEMP-MUSIC) and 9.1 dB (AR model). Among these four techniques, the dynamic range with the FFT is the largest, whereas that with the AR model is the smallest.

Figure 3 shows the ISAR images with the MEMP-MUSIC versus the subarray size. As the subarray size becomes larger, the resolution of MEMP-MUSIC improves, while its dynamic range becomes smaller, as expected. Although the results are not shown in this paper for the sake of brevity, we found that the other two high resolution techniques, the AR model and MUSIC, show very similar behavior to the MEMP-MUSIC.

Figure 4 presents the identification results as the subarray size is increased from 15 to 25 in increments of 5. In this figure, the vertical bars filled with black, dark gray, gray and white colors correspond to the results obtained from the FFT, AR, MUSIC and MEMP-MUSIC, respectively. Plots of the correct identification rates versus the subarray size are presented in Figure 4(a), and the associated standard deviations are given in Figure 4(b). As shown in Figure 4, the three high resolution techniques exhibit decreasing correct identification rates with increasing subarray size. Among the three techniques, the AR model has the most inferior results, while the other two have relatively high correct identification rates, because the ISAR images obtained from the AR model have very high sidelobes on the background and, thus, the lowest dynamic range, as shown in Figure 2. However, it is clearly revealed in Figure 4 that the traditional FFT method with wideband RCS data guarantees the most reliable

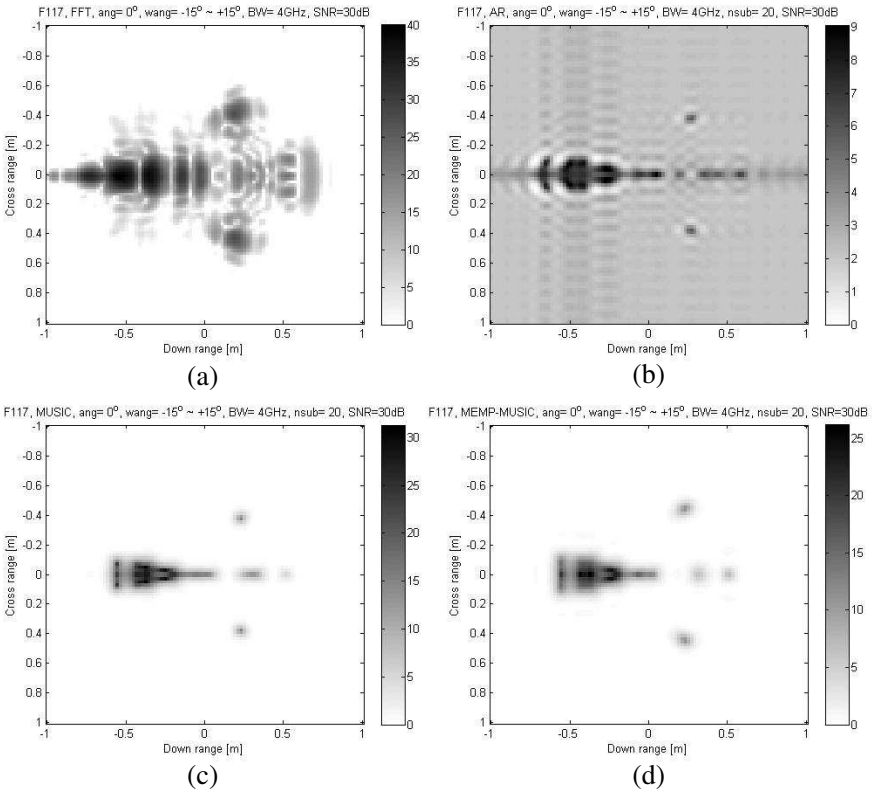

Figure 2. ISAR images whose frequency bandwidth is 4 GHz and angular region is 30° ($-15 \sim +15°$). (a) ISAR image via FFT. (b) ISAR image via AR model. (c) ISAR image via MUSIC. (d) ISAR image via MEMP-MUSIC.

identification performance. It should be noted that the FFT method has the most inferior resolution capability, but the most superior dynamic range among the four techniques, as shown in Figure 2. This suggests that the dynamic range as well as the resolution of an ISAR image is essential for successful target identification. If the resolution capability is guaranteed by wideband measurements, then the dynamic range has an important effect on the final identification accuracy.

Figure 5 shows the computation times of the four methods versus the subarray size. As expected, the FFT is the most efficient in terms of the computation, while the other three methods consume significant amounts of computation time compared to the FFT, because they require the time-consuming eigen-decomposition of the covariance matrix. Since the subarray size determines the size of the covariance

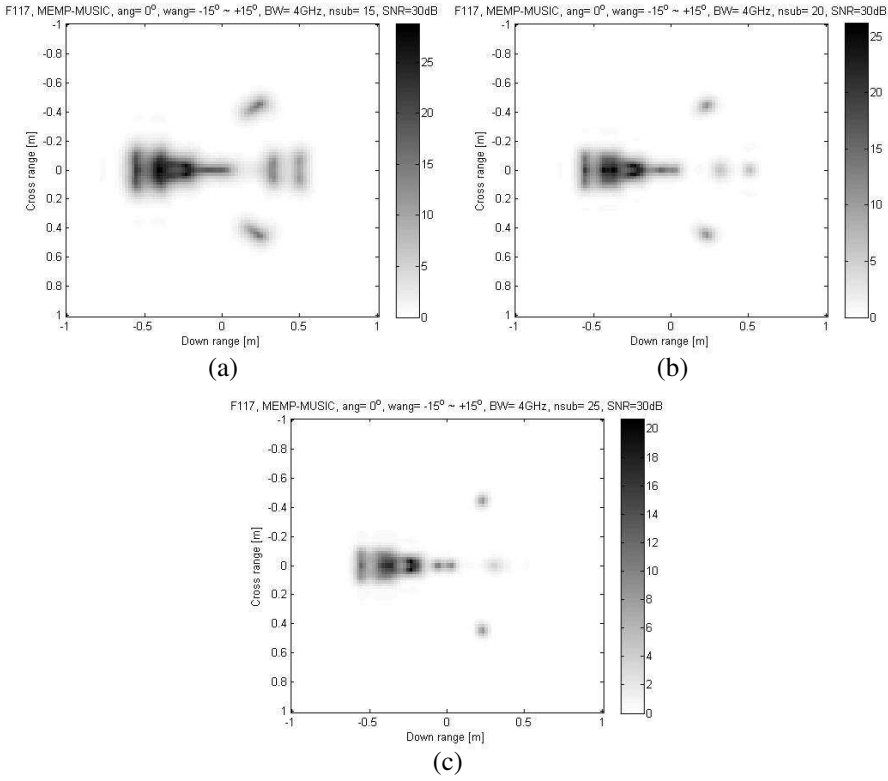

Figure 3. ISAR images using the MEMP-MUSIC vs. subarray size. (a) Subarray size = 15. (b) Subarray size = 20. (c) Subarray size = 25.

matrix, the computation time increases as the subarray size increases, as shown in Figure 5.

As a result, if sufficient resolution capability is guaranteed by wideband RCS data for a target, the traditional FFT is the most promising ISAR imaging algorithm for target identification, due to its large dynamic range and small computation time. In contrast, high resolution spectral estimation techniques can provide high resolution ISAR images at the expense of additional computation time, but their smaller dynamic ranges lead to the degradation of the identification performance, even with their improved resolution capability.

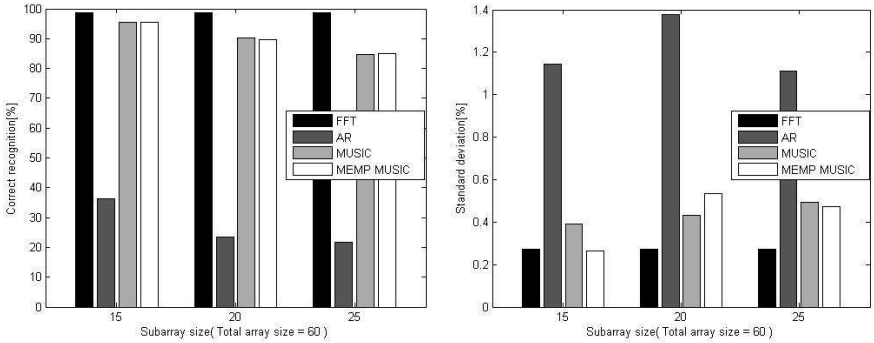

Figure 4. Average correct identification rate and standard deviation vs. subarray size using ISAR images of the data whose frequency bandwidth is 4 GHz and angular region is 30° (−15° ∼ +15°). (a) Average correct identification rates. (b) Standard deviations.

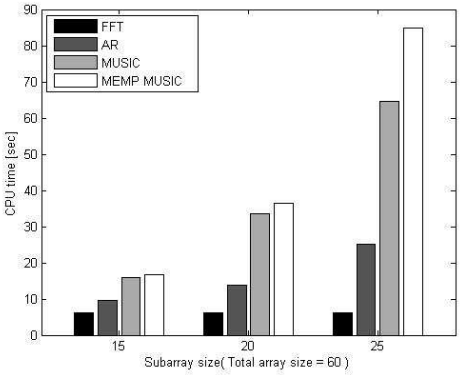

Figure 5. Average computation time for generating an ISAR image vs. subarray size.

3.2. Experiment II — Identification Using Narrowband Data

In this experiment, the RCS data with narrow bandwidth-angular sectors were used to generate the training and testing ISAR images. Their frequency bandwidth and angular sector were chosen as 2 GHz (9.3 GHz ∼ 11.3 GHz) and 10° (−5° ∼ +5°), respectively, corresponding to half the amount of data in Experiment I. Since the maximum size of the target models is about 1 m, the target response

corresponds to only about 13 range bins in the HRR profile domain with a narrow frequency bandwidth of 2 GHz, yielding 125 MHz against an actual target of length 16 m. As in Experiment I, an AWGN of 30 dB was added to the measured RCS data. However, the number of interpolated samples was decreased to $M = N = 30$, due to the reduced frequency bandwidth and angular sector. This ensures that the spatial frequency increments, Δf_x and Δf_y, in Experiment I with wideband RCS data, and those in Experiment II with narrowband RCS data are nearly identical. Then, the FFT, AR model, MUSIC and MEMP-MUSIC techniques for ISAR imaging were applied to these narrow frequency bandwidth-angular sector RCS data.

Figure 6 shows the ISAR images of the F117 scaled model obtained

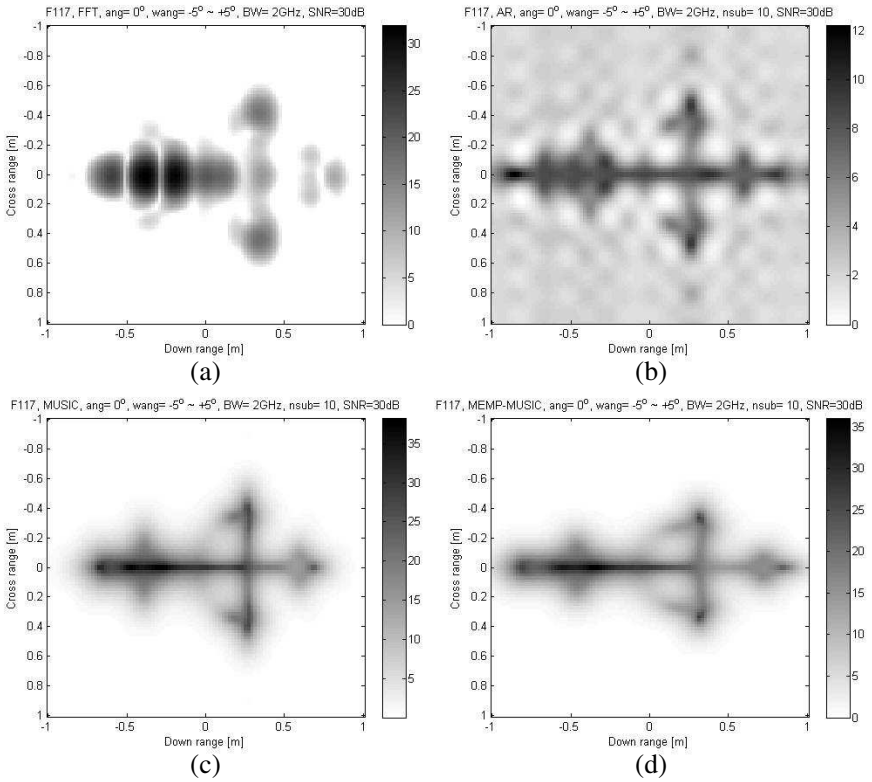

Figure 6. ISAR images of the data whose frequency bandwidth is 2 GHz and angular sector is 10° ($-5° \sim +5°$). (a) ISAR image using the FFT. (b) ISAR image using the AR model. (c) ISAR image using the MUSIC. (d) ISAR image using the MEMP-MUSIC.

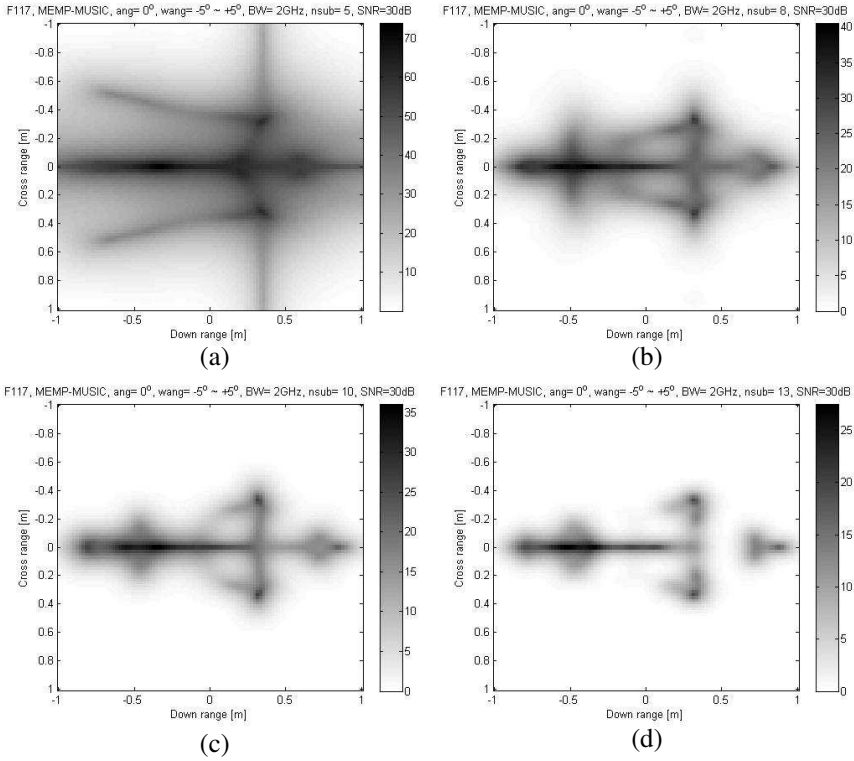

Figure 7. ISAR images using the MEMP-MUSIC vs. the subarray size. (a) Subarray size = 5. (b) Subarray size = 8. (c) Subarray size = 10. (d) Subarray size = 13.

using the various spectral estimation techniques with the narrow bandwidth RCS data. In Figure 6, the subarray size was selected as 10, i.e., about one-third of the full aperture size, $M = N = 30$. With the narrow band RCS data, the three high resolution techniques, as well as the FFT technique, provide degraded resolution ISAR images, as predicted. Even with this degraded resolution due to the reduced bandwidth, the high resolution techniques still show more improved resolution than the FFT. In terms of the dynamic range, the benefits of high resolution techniques against FFT are evident with the exception of AR model. It should be noted that in Experiment I, the FFT was shown to have a higher dynamic range than the high resolution PSD estimators. However, in the case of the narrow band RCS data, the high resolution techniques are able to provide more improved ISAR images in the framework of both the resolution and dynamic range.

Figure 7 shows the ISAR images obtained using the MEMP-MUSIC with various subarray sizes. As outlined in Experiment I, as the subarray size increases, the resolution capability of the ISAR image becomes more improved, while its dynamic range is deteriorated, and vice versa.

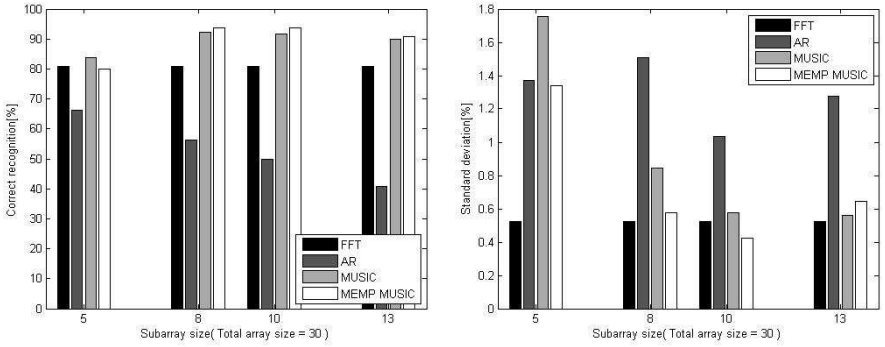

(a) (b)

Figure 8. Average correct identification rate and standard deviation vs. subarray size using ISAR images of the data whose frequency bandwidth is 2 GHz and angular sector is 10° ($-5° \sim +5°$). (a) Average correct identification rates. (b) Standard deviations.

Figure 8 presents the identification results obtained when the subarray size is 5, 8, 10 and 13. In this figure, the vertical bars filled with black, dark gray, gray and white colors correspond to the results obtained from the FFT, AR model, MUSIC and MEMP-MUSIC, respectively. The plots of the correct identification rates versus subarray size are presented in Figure 8(a), and the associated standard deviations are given in Figure 8(b). In contrast to the results obtained in Experiment I, the two high resolution techniques, such as viz. MUSIC and MEMP-MUSIC, show higher correct identification rates than the FFT against all of the subarray sizes considered. The improvements of the resolution as well as and dynamic range of afforded by MUSIC and MEMP-MUSIC compared to the FFT, as shown in Figure 6, lead to high identification outcomes, as shown in Figure 8.

It can be seen in Figure 8 that three methods, viz. the FFT, MUSIC, and MEMP-MUSIC, have relatively low and similar identification results when the subarray size is small. However, as the subarray size is increased (i.e., 8 and 10), the identification performances of MUSIC and MEMP-MUSIC improve, and, thus, they significantly outperform the FFT by more than 10%. This comes from

the fact that the enhancement of the resolution plays an important role in the identification accuracy when the subarray size is small. However, further increasing the subarray size to 13 gives rise to a slight degradation of the identification performance. This suggests that the dynamic range rather than the resolution comes to have a predominant effect on the identification performance when the subarray size is large enough to provide ISAR images with sufficient resolution. Therefore, subarray sizes of about one-quarter, i.e., 8, or one-third, i.e., 10, of the full aperture length, $M = N = 30$, are adequate for target identification with narrowband RCS data.

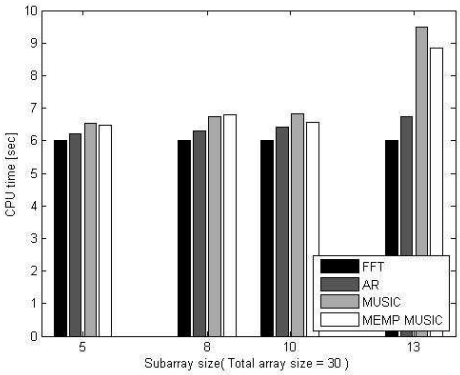

Figure 9. Average computation time vs. subarray size.

Figure 9 shows the variation of the average computation times of the four ISAR imaging methods with the subarray size. There is nearly no time difference between the FFT and the three high resolution techniques when the subarray size is relatively small, viz. 5, 8, and 10. The dimension of the covariance matrix depends on the subarray size, and, thus, with the narrowband RCS data, the computational efficiency of the high resolution PSD estimators becomes comparable to that of the FFT, especially for small sized subarrays.

In order to find an optimal subarray size at low SNR level, the measured data was contaminated by an AWGN of 10 dB. Other parameters except the SNR are same as those used in the previous experiment at high SNR.

Figure 10 shows the identification results obtained when the subarray size is 5, 8, 10 and 13. With lower SNR, the identification performances of four methods are degraded as expected. The plots of the correct identification rates versus subarray sizes are presented in Figure 10(a), and the associated standard deviations are given in Figure 10(b). The identification rates at subarray size of 8

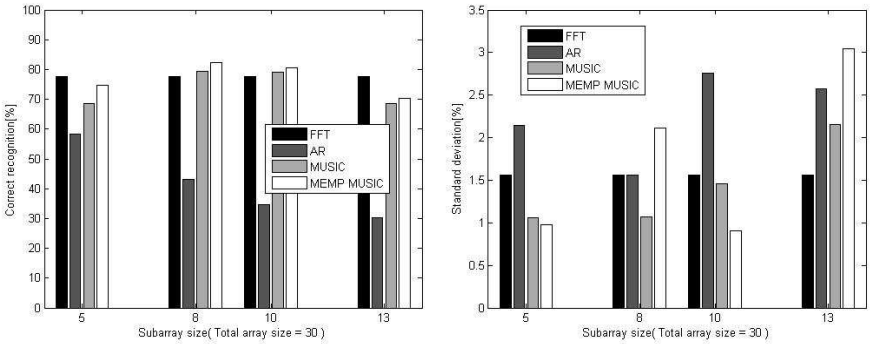

(a) (b)

Figure 10. Average correct identification rate and standard deviation vs. subarray size using ISAR images of the data whose frequency bandwidth is 2 GHz and angular sector is 10° ($-5^\circ \sim +5^\circ$). (a) Average correct identification rates. (b) Standard deviations.

and 10 outperform those at other subarray sizes. Also, the graph of identification performances versus the subarray size show similar behavior as in the case of high SNR in Figure 8. It can be clearly revealed that subarray sizes of about one-quarter, i.e., 8, or one-third, i.e., 10, of the full aperture length, $M = N = 30$, are adequate for target identification with narrowband RCS data even at low SNR.

Summarizing the above results, high resolution techniques including MUSIC and MEMP-MUSIC may significantly outperform the traditional low-resolution FFT method with narrowband RCS data. The identification performance is affected not only by the resolution, but also by the dynamic range of the ISAR images, as was discovered in Experiment I. In other words, a large subarray size for high resolved ISAR images does not always lead to the improvement of the identification accuracy for high resolution ISAR imaging techniques other than the FFT. In addition, the computational efficiency of the time-consuming high resolution techniques approaches that of the FFT technique without any loss of identification performance, especially for relatively small sized subarrays, i.e., 8 and 10. With the above extensive observations on the relations among the identification outcomes, resolution, dynamic range and computation time, it is evident that in the case of MUSIC and MEMP-MUSIC with narrowband data, a subarray size of about one-quarter of the full aperture size is adequate to achieve high correct identification rates with a minimal increase in the computational complexity.

4. CONCLUSION

In this paper, we presented the experimental results and associated analyses conducted for the purpose of investigating the performance of various ISAR imaging techniques, including high resolution spectral estimation techniques, as well as the conventional Fourier transform, in the framework of target identification. With wideband RCS data, the Fourier transform with lower resolution was shown to give more promising identification performance than the high resolution spectral estimation techniques, because the Fourier transform can provide ISAR images with more improved, i.e., larger, dynamic ranges. This suggests that the traditional Fourier transform is the most promising candidate for ISAR imaging with advanced radar systems having a large frequency bandwidth.

On the other hand, the high resolution spectral estimation techniques, except for the AR model, were better than the Fourier transform with the narrowband RCS data, because the Fourier transform results in poor resolution ISAR images for target identification. The high resolution techniques were superior to the Fourier transform in terms of both the resolution and dynamic ranges of the ISAR images. Furthermore, they are very efficient in terms of the computation time, due to their decreased subarray sizes. The optimum subarray size for high resolution ISAR imaging techniques was shown to be about one-quarter of the full aperture length, in terms of the target identification and computational complexity, because the identification performance depends not only on the resolution, but also on the dynamic range of the ISAR images. This also implies that high resolution spectral estimation techniques can be a cost-effective solution for ISAR imaging with traditional imaging radars having narrow frequency bandwidths, for example, less than 150 MHz.

ACKNOWLEDGMENT

This work was supported by the Yeungnam University research grants in 2010.

REFERENCES

1. Li, H. J. and V. Chiou, "Aerospace target identification-comparison between the matching score approach and the neural network approach," *Journal of Electromagnetic Waves and Applications*, Vol. 7, No. 6, 873–893, 1993.

2. Kim, K.-T., D.-K. Seo, and H.-T. Kim, "Efficient radar target recognition using the MUSIC algorithm and invariant features," *IEEE Transactions on Antennas and Propagation*, Vol. 50, No. 3, 325–327, Mar. 2002.
3. Li, H. J. and S. H. Yang, "Using range profiles as feature vectors to identify aerospace targets," *IEEE Transactions on Antennas and Propagation*, Vol. 41, 261–268, Mar. 1993.
4. Musman, S., D. Kerr, and C. Bachmann, "Automatic recognition of ISAR ship images," *IEEE Transactions on Aerospace and Electronic Systems*, Vol. 32, 1392–1404, Oct. 1996.
5. Kim, K.-T., D.-K. Seo, and H.-T. Kim, "Efficient classification of ISAR images," *IEEE Transactions on Antennas and Propagation*, Vol. 53, 1611–1621, May 2005.
6. Li, H. J. and K. M. Li, "Application of wavelet transform in target identification," *Progress In Electromagnetics Research*, Vol. 12, 57–73, 1996.
7. Seo, D.-K., K.-T. Kim, I.-S. Choi, and H.-T. Kim, "Wide-angle radar target recognition with subclass concept," *Progress In Electromagnetics Research*, Vol. 44, 231–248, 2004.
8. Jeong, J.-H., H.-T. Kim, and K.-T. Kim, "Comparisons of four feature extraction approaches based on fisher's linear discriminant criterion in radar target recognition," *Journal of Electromagnetic Waves and Applications*, Vol. 21, No. 2, 251–265, Jan. 2007.
9. Park, S.-H., K.-K. Park, J.-H. Jung, H.-T. Kim, and K.-T. Kim, "Construction of training database based on high frequency RCS prediction methods for ATR," *Journal of Electromagnetic Waves and Applications*, Vol. 22, No. 5-6, 693–703, 2008.
10. Rothwell, E., D. P. Nyquist, K. M. Chen, and B. Drachman, "Radar target discrimination using the extinction-pulse technique," *IEEE Transactions on Antennas and Propagation*, Vol. 33, 929–937, Sep. 1985.
11. Chen, K. M., D. P. Nyquist, E. J. Rothwell, L. L. Webb, and B. Drachman, "Radar target discrimination by convolution of radar returns with extinction pulses and single-mode extraction signals," *IEEE Transactions on Antennas and Propagation*, Vol. 34, 896–904, Jul. 1986.
12. Moony, J. E., Z. Ding, and L. S. Riggs, "Robust target identification in white Gaussian noise for ultra wide-band radar systems," *IEEE Transactions on Antennas and Propagation*, Vol. 46, 1817–1823, Dec. 1998.
13. Toribio, R., J. Saillard, and P. Pouliguen, "Identification of

radar targets in resonance zone: E-pulse techniques," *Progress In Electromagnetics Research*, Vol. 43, 39–58, 2003.

14. Moghaddar, A. and E. K. Walton, "Time-frequency distribution analysis of scattering from waveguide cavities," *IEEE Transactions on Antennas and Propagation*, Vol. 41, 677–680, May 1993.
15. Trintinalia, L. C. and H. Ling, "Interpretation of scattering phenomenology in slotted waveguide structures via time-frequency processing," *IEEE Transactions on Antennas and Propagation*, Vol. 43, 1253–1261, Nov. 1995.
16. Kim, H. and H. Ling, "Wavelet analysis of radar echo from finite-sized targets," *IEEE Transactions on Antennas and Propagation*, Vol. 41, 200–207, Feb. 1993.
17. Lazarov, A. D., M. Martorella, and C. Minchev, "Three dimensional Barker's ISAR signal and image reconstruction," *IEEE Radar Conference, RADAR'08*, 1–6, Rome, Italy, May 26–30, 2008.
18. Jeong, H.-R., H.-T. Kim, and K.-T. Kim, "Application of subarray averaging and entropy minimization algorithm to stepped-frequency ISAR autofocus," *IEEE Transactions on Antennas and Propagation*, Vol. 56, No. 4, 1144–1154, Apr. 2008.
19. Park, S.-H., K.-K. Park, J.-H. Jung, H.-T. Kim, and K.-T. Kim, "ISAR imaging of multiple targets using edge detection and hough transform," *Journal of Electromagnetic Waves and Applications*, Vol. 22, No. 2–3, 365–373, 2008.
20. Park, S.-H., H.-T. Kim, and K.-T. Kim, "Stepped-frequency isar motion compensation using particle swarm optimization with an island model," *Progress In Electromagnetics Research*, Vol. 85, 25–37, 2008.
21. Choi, G.-G., S.-H. Park, H.-T. Kim, and K.-T. Kim, "ISAR imaging of multiple targets based on particle swarm optimization and hough transform," *Journal of Electromagnetic Waves and Applications*, Vol. 23, 1825–1834, 2009.
22. Park, S.-H., H.-T. Kim, and K.-T. Kim, "Segmentation of ISAR images of targets moving in formation," *IEEE Transactions on Geoscience and Remote Sensing*, Vol. 48, No. 4, Apr. 2010.
23. Cao, P., M. Xing, G. Sun, Y. Li, and Z. Bao, "Minimum entropy via subspace for ISAR autofocus," *IEEE Geoscience and Remote Sensing Letters*, Vol. 7, 205–209, 2010.
24. Stoica, P. and R. L. Moses, *Introduction to Spectral Analysis*, Prentice-Hall, 1997.
25. Barabell, A. J., "Improving the resolution performance of

eigenstructure-based direction-finding algorithms," *Proceedings of the International Conference on Acoustics, Speech, and Signal Processing*, 336–339, Boston, MA, 1983.

26. Roy, R. and T. Kailath, "ESPRIT-estimation of signal parameters via rotational invariance techniques," *IEEE Transactions on Acoustics, Speech and Signal Processing*, Vol. 37, 984–995, Jul. 1989.
27. Gupta, I. J., "High resolution radar imaging using 2-D linear prediction," *IEEE Transactions on Antennas and Propagation*, Vol. 42, 31–37, Jan. 1994.
28. Kim, K.-T., S.-W. Kim, and H.-T. Kim, "Two-dimensional ISAR imaging using full polarization and super-resolution processing techniques," *IEE Proceedings Radar, Sonar, and Navigation*, Vol. 145, 240–246, Aug. 1998.
29. Odendaal, J. W., E. Barnard, and C. W. I. Pistorius, "Two-dimensional superresolution radar imaging using the MUSIC algorithm," *IEEE Transactions on Antennas and Propagation*, Vol. 42, 1386–1391, Oct. 1994.
30. Hua, Y., "Estimating two-dimensional frequencies by matrix enhancement and matrix pencil," *IEEE Transactions on Signal Processing*, Vol. 40, 2267–2280, Sep. 1992.
31. Duda, R. O., P. E. Hart, and D. G. Stork, *Pattern Classification*, 2nd Edition, John Wiley & Sons, Inc., 2001.
32. Theodoridis, S. and K. Koutroumbas, *Pattern Recognition*, Academic Press, 1999.
33. Lee, K.-C., J.-S. Ou, and M.-C. Fang, "Application of svd noise-reduction technique to PCA based radar target recognition," *Progress In Electromagnetics Research*, Vol. 81, 447–459, 2008.
34. Huang, C.-W. and K.-C. Lee, "Application of ica technique to PCA based radar target recognition," *Progress In Electromagnetics Research*, Vol. 105, 157–170, 2010.